

Co-diffusion of hydrogen and oxygen for dense oxyhydride synthesis

Masaya Fujioka^{1,2*}, Mihiro Hoshino², Suguru Iwasaki³, Katsuhiro Nomura¹, Aman Sharma¹, Mineyuki Hattori⁴, Reina Utsumi⁵, Yuki Nakahira⁵, Hiroyuki Saitoh⁵

¹ Innovative Functional Materials Research Institute, National Institute of Advanced Industrial Science and Technology (AIST), 4-205 Sakurazaka, Moriyama-ku, Nagoya, Aichi 463-8560, Japan

² Research Institute for Electronic Science, Hokkaido University, Kita 20, Nishi10, Kita-ku, Sapporo, Hokkaido 001-0020, Japan

³ Department of Industrial Chemistry, Faculty of Engineering, Tokyo University of Science, 6-3-1 Niijyuku Katsushika, Tokyo, 125-8585, Japan

⁴ Research Institute for Material and Chemical Measurement, National Metrology Institute of Japan (NMIJ), National Institute of Advanced Industrial Science and Technology (AIST), Tsukuba, Ibaraki 305-8565, Japan

⁵ National Institutes for Quantum Science and Technology (QST), 1-1-1 Kouto, Sayo, Hyogo 679-5148, Japan

* E-mail: m.fujioka@aist.go.jp

KEYWORDS. Oxyhydride, Diffusion, Electric conductivity, High pressure, Neutron diffraction, NMR

Abstract

Oxyhydrides are gaining attention for their diverse functionality. However, evaluating electron, ion, and phonon transport properties and comprehending their mechanism remains challenging due to the difficulty in oxyhydride synthesis involving the trade-off between achieving density sintering and preventing hydrogen evolution. High-temperature treatments, often required to reduce intergranular resistance, typically cause hydrogen evolution before sufficient sintering. Instead of a post-annealing process aiming for strong chemical connections between oxyhydride particles, this research demonstrates a novel synthesis technique that converts pre-sintered bulk oxides into oxyhydrides while preserving the dense state. The process employs a high-pressure diffusion control method, facilitating the co-diffusion of hydride and oxide ions.

Hydrogen is a unique element that can flexibly change its chemical state from monovalent cation to monovalent anion, depending on the surrounding environment in the crystal structure. "Oxyhydrides," including a monovalent hydride (H^-) and a divalent oxide ion (O^{2-}) in the same crystal structure, have attracted attention due to their various functionalities, such as superconductivity¹, solid-state ionics², thermoelectric conversion properties³, catalytic properties⁴⁻⁵, and Photochromic properties⁶⁻⁷.

Some oxyhydrides can be synthesized through simple hydrogen reduction⁸, but in many cases, much stronger reducing conditions using metal or saline hydrides, such as CaH_2 , are required. The synthesis process of mixing with these hydrogen sources and sintering at a low temperature in an evacuated tube successfully creates various oxyhydrides⁹⁻¹⁴. By-product oxides via this reaction, such as CaO , are removed by acid treatment, and powdered oxyhydrides are available. Hydrogen with weak bonding is easily released from the crystal structure, so the hydrogen evolution temperatures in perovskite oxyhydrides $\text{ATiO}_{3-x}\text{H}_x$ ($\text{A} = \text{Ba}, \text{Sr}, \text{Ca}$) have been reported to be as low as 500°C ¹¹. Since these perovskite oxides require high temperatures treatment at approximately over 1000°C to sinter densely, it is challenging to evaluate essential transport properties, ignoring the intergranular resistance. Indeed, the $\text{BaTiO}_{3-x}\text{H}_x$ epitaxial thin films showed 10^6 times lower resistivity at room temperature than that of pelletized samples^{12, 15}; these films without grain boundary can be prepared by low-temperature treatment with embedding in CaH_2 , leading to negligible intergranular resistance¹⁵⁻¹⁶. To achieve bulk polycrystalline oxyhydride with significantly reduced intergranular resistance, similar to epitaxial thin films, and delve deeper into the physical properties, such as electron, ion, or phonon transportations, we need a technology that solves the challenge of dense sintering without hydrogen evolution. Our strategy in this study is to convert already sintered dense oxide into oxyhydride while keeping the dense state by co-diffusion of hydride and oxide ions, rather than the post-annealing process aimed at creating strong chemical connections between oxyhydride particles.

In the case of nm-ordered thin films, such substitution easily proceeds sufficiently due to the interdiffusion of oxygen and hydrogen at the contact interface with the hydrogen source. However, even if a similar treatment is applied to a mm-ordered dense bulk oxide, the substitution occurs only on the outermost surfaces, making it impossible to introduce hydride into the interior homogeneously. This research developed a new process for oxyhydrides by supplying hydrogen and extracting oxygen from the opposite side, leading to the co-diffusion in a specific direction throughout the bulk polycrystal.

Some synthesis methods utilizing anisotropic diffusion have been reported¹⁷⁻¹⁹. They are based on the same strategy and can modulate the chemical composition by introducing,

extracting, and exchanging weakly bonded elements in the crystal structure, focusing on the differences in the chemical bonding strength among constituent elements. For instance, the anisotropic diffusion control (ADC) method can promote the diffusion of elements by intentionally creating a chemical potential gradient, allowing it to work effectively even for electron-conductive compounds where ion control is impossible using an electric field due to the electrostatic shielding effect^{18,20}. Furthermore, high-pressure diffusion control (HPDC) is the method that makes ADC possible under high pressure¹⁷.

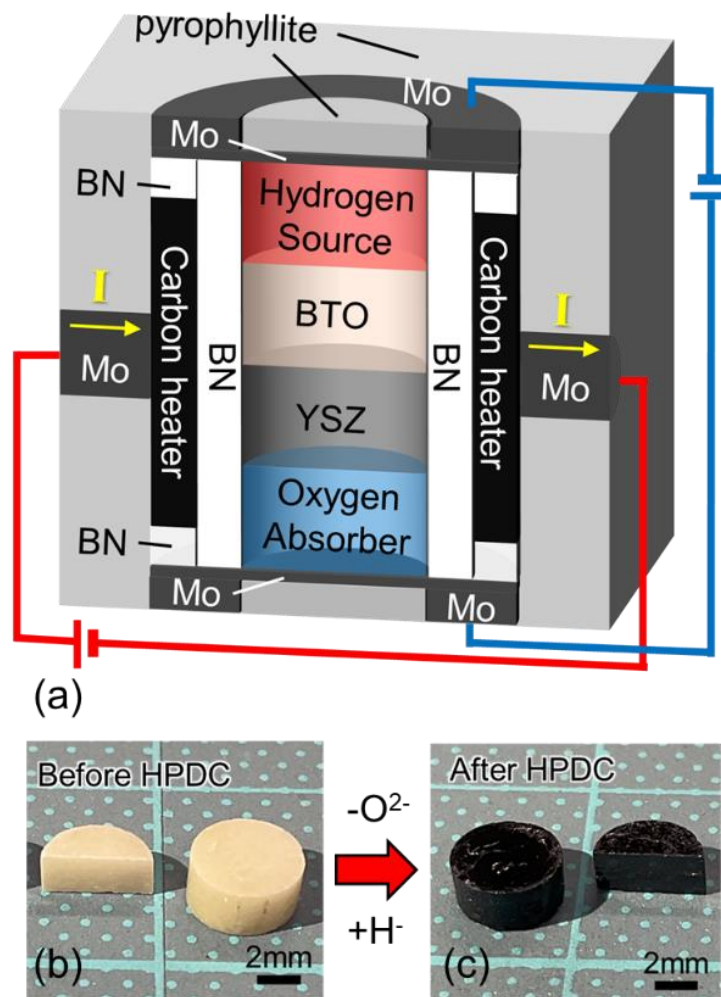


Figure 1. (a) schematic illustration of HPDC. Optical images of BTO (b) before and (c) after treatment.

Figure 1(a) is a schematic illustration of a cross-section of HPDC. By modifying the cubic-type high-pressure cell, it is possible to control temperature, pressure, and voltage simultaneously. The temperature can be adjusted using the left and right Mo electrodes, and the voltage applied to the sample space can be controlled using the upper and lower Mo electrodes. The pressure ensures good chemical and physical contact between and within compounds in sample space, compensating for gradual volume change caused by the elemental migration²¹. The sample space consisted of a stacked structure of a hydride source, BaTiO₃ (BTO), yttria-stabilized zirconia (YSZ), and an oxygen absorber, as shown in Figure 1(a). BTO polycrystals were comprised of densely connected grains formed by sintering at 1300°C for 20 h. Various candidates for hydrogen sources, such as NaH, MgH₂, CaH₂, and LaH₃, and oxide absorbers, such as Ti, Zr, or Ca powders, were considered, but a combination of MgH₂ and Ti was adopted in this study. Under 1 GPa, the temperature was raised at 50°C/min to 530°C, then increased by 4°C/min to 650°C, and treated at 650°C for 40 hours. As shown in Figure 1(b) and 1(c), the co-diffusion of hydride and oxide ions progressed in the densely sintered BTO, forming BaTiO_{3-x}H_x (BTOH) with a dark blue color (almost black) while maintaining its dense state. In this method, the hydride content in the sample can be roughly controlled by adjusting the amount of current flowing through the sample space, as shown in Figure S1.

When gradually increasing temperature under applying 5 V (Figure S2(a)), the current started to rise around 290°C, and a further increase was observed around 600°C; a two-step change in current behavior was evident according to temperature. The first increase is related to oxygen migration due to the oxygen absorption by Ti, and the second change is due to hydrogen diffusion derived from the decomposition of MgH₂. Figure S2(b) shows the in-situ observation of synchrotron x-ray diffraction measurements under high pressure at the BL14B1 experimental station of SPring-8, where the 002 peak intensity of Ti begins to change around 280°C at 1 GPa, corresponding to the first change in current. It is also known that MgH₂ decomposes around 630°C under 1 GPa²². Furthermore, Figure S3 shows the effects of the oxygen absorber and the voltage application on oxygen extraction. These results also support the oxygen migration starting from 280°C. The oxygen extraction from the bulk proceeds more homogeneously with voltage application, as shown in Figure S3(c). The details are provided in the supporting information (Section 3). Conversely, when the sample is treated with only a hydrogen source without an oxygen absorber, hydrogen substitution only occurs at the interface between the sample and the hydrogen source and hardly progresses throughout the sample.

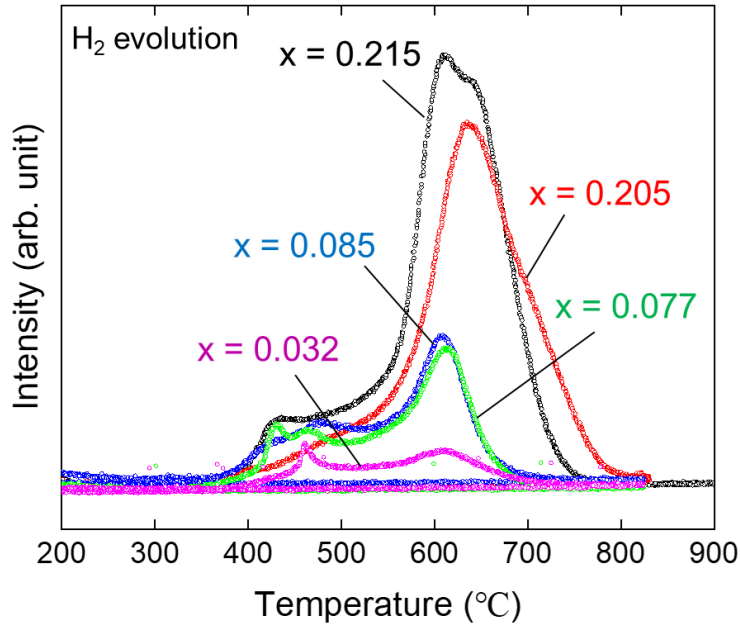


Figure 2. TPD-MS measurements for $\text{BaTiO}_{3-x}\text{H}_x$.

Figure 2 shows the temperature-programmed desorption mass spectrometry (TPD-MS) measurements for prepared BTOH. Although the obtained profiles consist of several peaks, the main peak appeared around 620°C . It clearly grows as the hydrogen concentration increases. The hydrogen evolution temperatures of $\text{ABO}_{3-x}\text{H}_x$ have generally been reported to be less than 500°C ,¹¹ when sintered with CaH_2 but increase to over 600°C with high-pressure treatment³. Such high-pressure treatments, including HPDC, may alter the chemical bonding state of hydrides, leading to an increase in hydrogen evolution temperature. In addition, nuclear magnetic resonance (NMR) measurements were performed to confirm the valence of substituted hydrogen in BTOH, as shown in Figure S4. Consistent with previous reports²³⁻²⁴, the peak corresponding to hydrogen inside the solid shifts from -1 ppm to -25 ppm as the hydrogen concentration increases.

Figure 3 shows the temperature dependence of the electrical resistivity for BTOH with different hydride concentrations using the same samples as Figure 2. The samples were cut into $4.2 \times 1.2 \times 0.5 \text{ mm}^3$ sizes. Change in hydrogen concentration along the thickness direction was also investigated and considered to have an almost uniform hydrogen distribution, as shown in Figure S5. The resistivity slightly increased at lower temperatures in the samples with $x = 0.032$, 0.077 , and 0.085 , but as the hydrogen concentration reached around $x = 0.2$, the electrical resistivity decreased linearly and showed metallic behavior. When $x = 0.215$, the resistivity at 300 K was $1.6 \times 10^{-3} \Omega\text{cm}$,

resulting in conduction properties close to those of reported epitaxial thin films ($0.8 \times 10^{-3} \Omega\text{cm}$). Thus, the HPDC demonstrated that dense bulk oxyhydrides with significantly reduced intergranular resistance can be achieved and that their hydrogen concentrations can be systematically tuned by monitoring current.

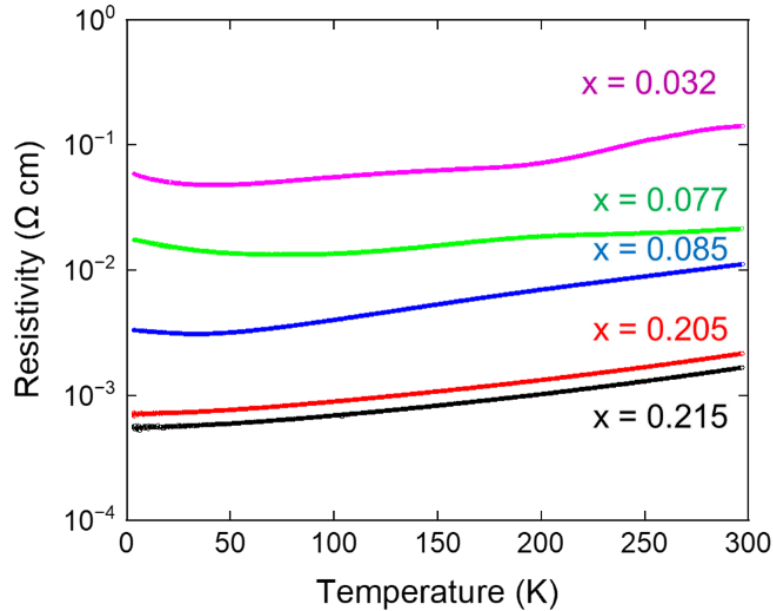


Figure 3. Temperature dependence of resistivity for $\text{BaTiO}_{3-x}\text{H}_x$ with different hydride concentrations.

Structural analyses for the samples with $x = 0.077$ and 0.215 were performed using Rietveld refinements of powder neutron diffraction²⁵. It is known that the tetragonal structure of BTO approaches the cubic structure with hydrogen substitution²⁶; the same behavior was confirmed in the case of HPDC, as shown in Figure S6. Three structural models were assumed in this study: cubic phase, tetragonal phase, and a mixed phase of both. The R factors decreased for the tetragonal structure than for the cubic structure, and the two-phase fitting confirmed a further reduction, in both cases of $x = 0.077$ and $x=0.215$. The estimated hydrogen contents were $x = 0.065$ and $x = 0.213$, respectively, which were comparable to the results obtained by TPD-MS. The amount of oxygen vacancies was estimated to be $x = 0.081$ and $x = 0.228$, suggesting that most of the oxygen vacancies are occupied by hydride. Detailed results are summarized in Figure S7 and Tables S1 and S2. Figure 4 shows the results of the maximum-entropy method (MEM) analysis obtained from the neutron diffraction data for the sample with $x = 0.215$, visualizing the negative scattering density of H and Ti. For the cubic structure (Figure 4(a)), these negative scattering densities appeared at 3d and 12i sites, suggesting hydrogen

occupation at their sites. However, they were not confirmed for the tetragonal structure (Figure 4(b)). On the other hand, the 3d site in the cubic structure disappeared in the two-phase model, though the negative scattering densities around the oxygen site remained. Therefore, this research also considered hydroxide formation using Rietveld analysis, assuming the additional hydrogen at the 12i site, and DFT calculations to search for the stable site of additional hydrogen²⁷⁻²⁹, as discussed in Figure S8 and Table S3. These structural analyses strongly suggest the formation of hydrides in oxide ion sites rather than protons in the hydroxyl group. Additionally, the crystal structure after HPDC approaches the cubic but does not achieve a completely cubic structure, which is consistent with the previous report²⁶.

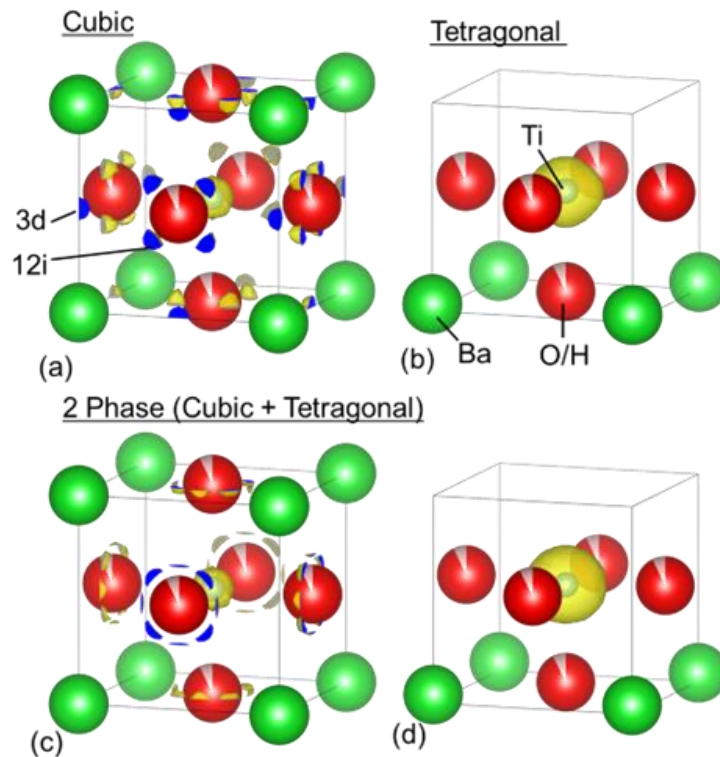


Figure 4. MEM analysis from neutron diffraction measurements of $\text{BaTiO}_{3-x}\text{H}_x$ ($x=0.215$) assuming (a) cubic, (b) tetragonal, and their mixed phases: (c) cubic and (d) tetragonal. The crystal structures were drawn using the visualization for electronic and structural analysis (VESTA).³⁰

The HPDC method partially exchanged oxide ions to hydride ions through co-diffusion and successfully converted BTO to BTOH while maintaining the densely sintered state. Such uniform substitution throughout the bulk poly-crystal, extending over several millimeters, is impossible by merely supplying hydride from the interface with the

hydrogen source. However, anisotropic co-diffusion, facilitated by the simultaneous extraction of oxide ions from the opposite side, makes this process possible, resulting in metallic conduction with reduced intergranular resistance.

Here, we propose four advantages of this method, highlighting its promising potential. First, no contamination occurs from the constituent elements of the hydrogen sources. Second, the high-density bulk oxyhydride enables the characterization of essential transport properties of electrons, ions, and phonons with reduced intergranular resistivity. Third, the method offers sufficient versatility and can be applied to various oxides, not just BTO. Fourth, this diffusion-based method should, in principle, be effective for single crystals as well as polycrystals. The creation of single crystals will greatly contribute to uncovering previously unknown physical and chemical aspects of oxyhydrides.

Acknowledgment

This work was supported by the Japan Science and Technology Agency (JST) CREST (Grant No. JPMJCR19J1), the Japan Society for the Promotion of Science (JSPS) (Grant Nos. 19H02420 and 24K01171). The synchrotron XRD measurements were supported by the QST Advance Characterization "Advanced Research Infrastructure for Materials and Nanotechnology in Japan (ARIM)" (Proposal Nos. JPMXP1222QS0114 and JPMXP1223QS0012) of the Ministry of Education, Culture, Sports, Science and Technology (MEXT). The synchrotron radiation X-ray diffraction experiments were performed using a QST experimental station at the QST beamline BL14B1 and SPring-8, with the approval of the Japan Synchrotron Radiation Research Institute JASRI (Proposal Nos. 2022B3682 and 2023A3682). The neutron diffraction measurements were performed at the beamline BL-20 in the Material and Life Science Experimental Facility (MLF) of the Japanese Proton Accelerator Research Complex (J-PARC) (No.2024A0301). Solid-state NMR measurements were supported by the AIST Nanocharacterization Facility (ANCF) in the Advanced Research Infrastructure for Materials and Nanotechnology (No. JPMXP1224AT5040) sponsored by the Ministry of Education, Culture, Sports, Science, and Technology (MEXT), Japan. We would like to express our gratitude to Ms. Masae Sawamoto, Research Institute for Electronic Science, Hokkaido University, Ms. Yukino Nishikubo, Innovative Functional Materials Research Institute, National Institute of Advanced Industrial Science and Technology for preparing the HPDC cells and providing insight that greatly assisted the research.

References

1. Iimura, S.; Matsuishi, S.; Sato, H.; Hanna, T.; Muraba, Y.; Kim, S. W.; Kim, J. E.;

- Takata, M.; Hosono, H., Two-dome structure in electron-doped iron arsenide superconductors. *Nat Commun* 2012, 3, 943.
2. Kobayashi, G.; Hinuma, Y.; Matsuoka, S.; Watanabe, A.; Iqbal, M.; Hirayama, M.; Yonemura, M.; Kamiyama, T.; Tanaka, I.; Kanno, R., Pure H- conduction in oxyhydrides. *Science* 2016, 351, 1314-1317.
3. He, X.; Nomoto, S.; Komatsu, T.; Katase, T.; Tadano, T.; Kitani, S.; Yoshida, H.; Yamamoto, T.; Mizoguchi, H.; Ide, K.; Hiramatsu, H.; Kawaji, H.; Hosono, H.; Kamiya, T., Hydride Anion Substitution Boosts Thermoelectric Performance of Polycrystalline SrTiO₃ via Simultaneous Realization of Reduced Thermal Conductivity and High Electronic Conductivity. *Advanced Functional Materials* 2023, 33, 2213144.
4. Tang, Y.; Kobayashi, Y.; Masuda, N.; Uchida, Y.; Okamoto, H.; Kageyama, T.; Hosokawa, S.; Loyer, F.; Mitsuhara, K.; Yamanaka, K.; Tamenori, Y.; Tassel, C.; Yamamoto, T.; Tanaka, T.; Kageyama, H., Metal-Dependent Support Effects of Oxyhydride-Supported Ru, Fe, Co Catalysts for Ammonia Synthesis. *Advanced Energy Materials* 2018, 8, 1801772.
5. Tang, Y.; Kobayashi, Y.; Tassel, C.; Yamamoto, T.; Kageyama, H., Hydride-Enhanced CO₂ Methanation: Water-Stable BaTiO_{2.4}H_{0.6} as a New Support. *Advanced Energy Materials* 2018, 8, 1800800.
6. Nafezarefi, F.; Schreuders, H.; Dam, B.; Cornelius, S., Photochromism of rare-earth metal-oxy-hydrides. *Appl Phys Lett* 2017, 111, 103903.
7. Colombi, G.; Cornelius, S.; Longo, A.; Dam, B., Structure Model for Anion-Disordered Photochromic Gadolinium Oxyhydride Thin Films. *The Journal of Physical Chemistry C* 2020, 124, 13541-13549.
8. Toriumi, H.; Kobayashi, G.; Saito, T.; Kamiyama, T.; Sakai, T.; Nomura, T.; Kitano, S.; Habazaki, H.; Aoki, Y., Barium Indate–Zirconate Perovskite Oxyhydride with Enhanced Hydride Ion/Electron Mixed Conductivity. *Chem Mater* 2022, 34, 7389-7401.
9. Nakamura, M.; Watanabe, H.; Akamatsu, H.; Fujii, K.; Yashima, M.; Hasegawa, G.; Inada, M.; Hayashi, K.; Maeda, K., Sn-Based Perovskite with a Wide Visible-Light Absorption Band Assisted by Hydride Doping. *Chem Mater* 2021, 33, 3631-3638.
10. Denis Romero, F.; Leach, A.; Moller, J. S.; Foronda, F.; Blundell, S. J.; Hayward, M. A., Strontium vanadium oxide-hydrides: "square-planar" two-electron phases. *Angew Chem Int Ed Engl* 2014, 53, 7556-7559.
11. Sakaguchi, T.; Kobayashi, Y.; Yajima, T.; Ohkura, M.; Tassel, C.; Takeiri, F.; Mitsuoka, S.; Ohkubo, H.; Yamamoto, T.; Kim, J.; Tsuji, N.; Fujihara, A.; Matsushita, Y.; Hester, J.; Avdeev, M.; Ohoyama, K.; Kageyama, H., Oxyhydrides of (Ca,Sr,Ba)TiO₃ perovskite solid solutions. *Inorg Chem* 2012, 51, 11371-11376.

12. Kobayashi, Y.; Hernandez, O. J.; Sakaguchi, T.; Yajima, T.; Roisnel, T.; Tsujimoto, Y.; Morita, M.; Noda, Y.; Mogami, Y.; Kitada, A.; Ohkura, M.; Hosokawa, S.; Li, Z.; Hayashi, K.; Kusano, Y.; Kim, J.; Tsuji, N.; Fujiwara, A.; Matsushita, Y.; Yoshimura, K.; Takegoshi, K.; Inoue, M.; Takano, M.; Kageyama, H., An oxyhydride of BaTiO₃ exhibiting hydride exchange and electronic conductivity. *Nat Mater* 2012, 11 (6), 507-511.
13. Helps, R. M.; Rees, N. H.; Hayward, M. A., Sr₃Co₂O_{4.33}H_{0.84}: an extended transition metal oxide-hydride. *Inorg Chem* 2010, 49, 11062-11068.
14. Hayward, M. A.; Cussen, E. J.; Claridge, J. B.; Bieringer, M.; Rosseinsky, M. J.; Kiely, C. J.; Blundell, S. J.; Marshall, I. M.; Pratt, F. L., The hydride anion in an extended transition metal oxide array: LaSrCoO₃H_{0.7}. *Science* 2002, 295, 1882-1884.
15. Yajima, T.; Kitada, A.; Kobayashi, Y.; Sakaguchi, T.; Bouilly, G.; Kasahara, S.; Terashima, T.; Takano, M.; Kageyama, H., Epitaxial thin films of ATiO₃-xH_x (A = Ba, Sr, Ca) with metallic conductivity. *J Am Chem Soc* 2012, 134, 8782-8785.
16. Yamamoto, T.; Yoshii, R.; Bouilly, G.; Kobayashi, Y.; Fujita, K.; Kususe, Y.; Matsushita, Y.; Tanaka, K.; Kageyama, H., An antiferro-to-ferromagnetic transition in EuTiO₃-xH_x induced by hydride substitution. *Inorg Chem* 2015, 54, 1501-1507.
17. Fujioka, M.; Hoshino, M.; Iwasaki, S.; Morito, H.; Kumagai, M.; Katsura, Y.; Zagarzusem, K.; Ono, M.; Nishii, J., High-Pressure Diffusion Control: Na Extraction from NaAlB₁₄. *Chem Mater* 2023, 35, 3008-3014.
18. Iwasaki, S.; Morito, H.; Komine, T.; Morita, K.; Shibuya, T.; Nishii, J.; Fujioka, M., A Novel Technique for Controlling Anisotropic Ion Diffusion: Bulk Single-Crystalline Metallic Silicon Clathrate. *Adv Mater* 2022, 34, 2106754.
19. Fujioka, M.; Wu, C.; Kubo, N.; Zhao, G.; Inoishi, A.; Okada, S.; Demura, S.; Sakata, H.; Ishimaru, M.; Kaiju, H.; Nishii, J., Proton-Driven Intercalation and Ion Substitution Utilizing Solid-State Electrochemical Reaction. *J Am Chem Soc* 2017, 139, 17987-17993.
20. Iwasaki, S.; Morito, H.; Hoshino, M.; Nishii, J.; Fujioka, M., 93 at.% of Na extraction from a Na₂₄Si₁₃₆ single crystal via anisotropic ion diffusion control method. *Journal of Solid State Chemistry* 2023, 324, 124082.
21. Iwasaki, S.; Hoshino, M.; Morito, H.; Kumagai, M.; Katsura, Y.; Nishii, J.; Fujioka, M., Effect of intergranular connectivity of NaAlB₁₄ on Na⁺ extraction. *Solid State Sciences* 2023, 144, 107308.
22. Fujioka, M.; Zagarzusem, K.; Iwasaki, S.; Sharma, A.; Watanabe, K.; Nakayama, R.; Momai, M.; Yamaguchi, Y.; Shimada, H.; Nomura, K.; Mizutani, Y.; Sumi, H.; Tanaka, M.; Jeem, M.; Hattori, M.; Saitoh, H.; Ozaki, T.; Nagao, M.; Nagashima, K., Hydrogen-Assisted Mg Intercalation into 2H-TaS₂. *J Am Chem Soc* 2024, 146, 34324-34332.
23. Guo, H.; Jaworski, A.; Ma, Z.; Slabon, A.; Bacsik, Z.; Nedumkandathil, R.;

- Haussermann, U., Trapping of different stages of BaTiO₃ reduction with LiH. *RSC Adv* 2020, 10, 35356-35365.
24. Nedumkandathil, R.; Jaworski, A.; Grins, J.; Bernin, D.; Karlsson, M.; Eklof-Osterberg, C.; Neagu, A.; Tai, C. W.; Pell, A. J.; Haussermann, U., Hydride Reduction of BaTiO₃ - Oxyhydride Versus O Vacancy Formation. *ACS Omega* 2018, 3, 11426-11438.
25. Oishi, R.; Yonemura, M.; Nishimaki, Y.; Torii, S.; Hoshikawa, A.; Ishigaki, T.; Morishima, T.; Mori, K.; Kamiyama, T., Rietveld analysis software for J-PARC. *Nuclear Instruments and Methods in Physics Research Section A: Accelerators, Spectrometers, Detectors and Associated Equipment* 2009, 600, 94-96.
26. Kanazawa, T.; Nishioka, S.; Yasuda, S.; Kato, D.; Yokoi, T.; Nozawa, S.; Kageyama, H.; Maeda, K., Influence of the Hydride Content on the Local Structure of a Perovskite Oxyhydride BaTiO₃-xHx. *The Journal of Physical Chemistry C* 2023, 127, 7546-7551.
27. Fujioka, M.; Jeem, M.; Sato, K.; Tanaka, M.; Morita, K.; Shibuya, T.; Takahashi, K.; Iwasaki, S.; Miura, A.; Nagao, M.; Demura, S.; Sakata, H.; Ono, M.; Kaiju, H.; Nishii, J., Intercalation on Transition Metal Trichalcogenides via a Quasi-Amorphous Phase with 1D Order. *Advanced Functional Materials* 2023, 33, 22087022.
28. Kresse, G.; Furthmuller, J., Efficient iterative schemes for ab initio total-energy calculations using a plane-wave basis set. *Phys Rev B Condens Matter* 1996, 54, 11169-11186.
29. Perdew, J. P.; Burke, K.; Ernzerhof, M., Generalized gradient approximation made simple. *Phys Rev Lett* 1996, 77, 3865-3868.
30. Momma, K.; Izumi, F., VESTA 3 for three-dimensional visualization of crystal, volumetric and morphology data. *J Appl Crystallogr* 2011, 44, 1272-1276.

Supporting information for

Co-diffusion of hydrogen and oxygen for dense oxyhydride synthesis

Masaya Fujioka^{1,2*}, Mihiro Hoshino², Suguru Iwasaki³, Katsuhiro Nomura¹, Aman Sharma¹, Mineyuki Hattori⁴, Reina Utsumi⁵, Yuki Nakahira⁵, Hiroyuki Saitoh⁵

¹ Innovative Functional Materials Research Institute, National Institute of Advanced Industrial Science and Technology (AIST), 4-205 Sakurazaka, Moriyama-ku, Nagoya, Aichi 463-8560, Japan

² Research Institute for Electronic Science, Hokkaido University, Kita 20, Nishi 10, Kita-ku, Sapporo, Hokkaido 001-0020, Japan

³ Department of Industrial Chemistry, Faculty of Engineering, Tokyo University of Science, 6-3-1 Niiyuku Katsushika, Tokyo, 125-8585, Japan

⁴ Research Institute for Material and Chemical Measurement, National Metrology Institute of Japan (NMIJ), National Institute of Advanced Industrial Science and Technology (AIST), Tsukuba, Ibaraki 305-8565, Japan

⁵ National Institutes for Quantum Science and Technology (QST), 1-1-1 Kouto, Sayo, Hyogo 679-5148, Japan

* E-mail: m.fujioka@aist.go.jp

KEYWORDS. Oxyhydride, Diffusion, Electric conductivity, High pressure, Neutron diffraction, NMR

Content

1. Treatment conditions of HPDC
2. Operand measurements and in-situ observations during the HPDC treatment
3. Effect of the oxygen absorber and applying voltage on oxygen extraction from BTO
4. NMR measurements
5. Change in hydrogen concentration along the thickness direction
6. XRD measurements
7. Rietveld refinement analyses of powder neutron diffraction
8. Possibility of OH formation
9. Method

1. Treatment conditions of HPDC

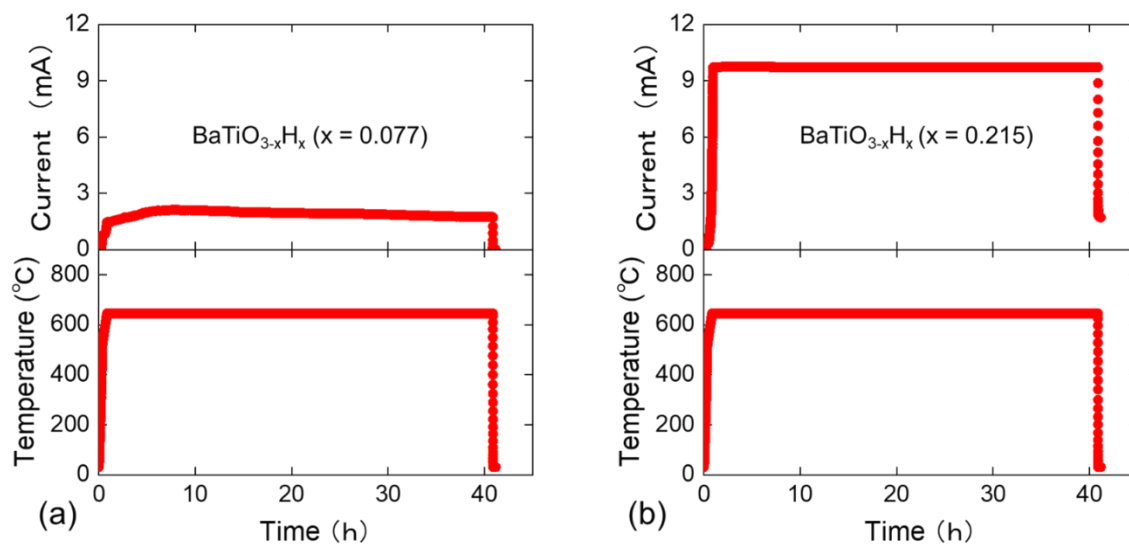


Figure S1. Treatment conditions of HPDC for (a) $\text{BaTiO}_{3-x}\text{H}_x$ ($x=0.077$) and (b) $\text{BaTiO}_{3-x}\text{H}_x$ ($x=0.215$).

2. Operand measurements and in-situ observations during the HPDC treatment

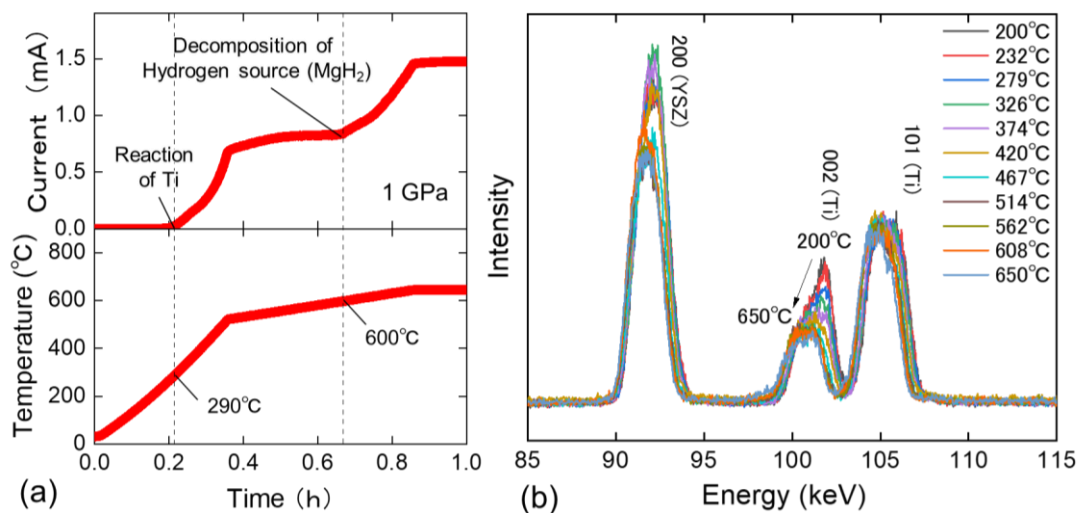


Figure S2. (a) Time and temperature dependence of current passed the sample space at 1 GPa. (b) In-situ observation of oxygen absorber using synchrotron x-ray diffraction from 200°C to 650°C under 1 GPa.

3. Effect of the oxygen absorber and applying voltage on oxygen extraction from BTO

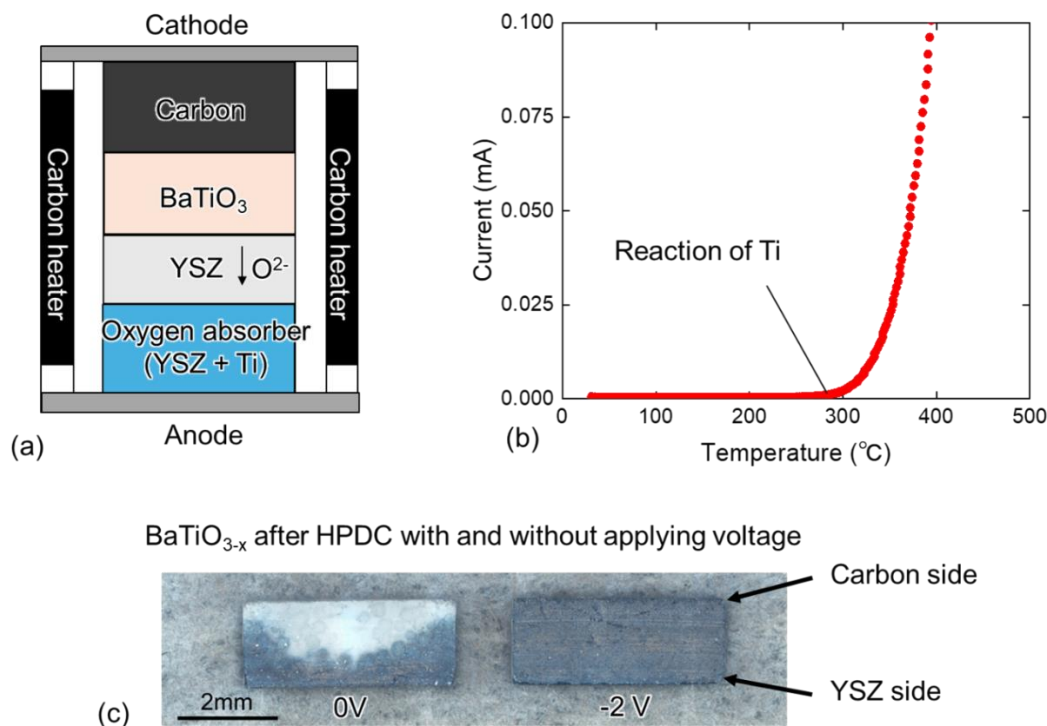


Figure S3. (a) The schematic illustration of sample space to investigate the oxygen extraction by Ti. (b) Temperature dependence of current passed sample space during the HPDC treatment. (c) The cross sections of optical images for the samples after HPDC treatment with and without voltage application.

The effect of the oxygen absorber and the application of voltage on oxide ion extraction was investigated. To eliminate the influence of MgH₂ during the HPDC process, the hydrogen source was replaced with carbon. The sample was held at 400°C for 20 hours, as treatments within the temperature range of 290°C and 600°C are known to promote oxygen absorption. As a result, a color change indicative of oxygen vacancies was observed, as shown in Figure S3(c). The formation of oxygen vacancies enhances electronic conductivity, which gradually reduces the contribution of the electric field as a driving force for oxide ion diffusion. Conversely, an electric field should be concentratedly applied in an area without oxygen vacancies. It may lead to more homogeneous oxygen extraction from the dense bulk material.

4. NMR measurements

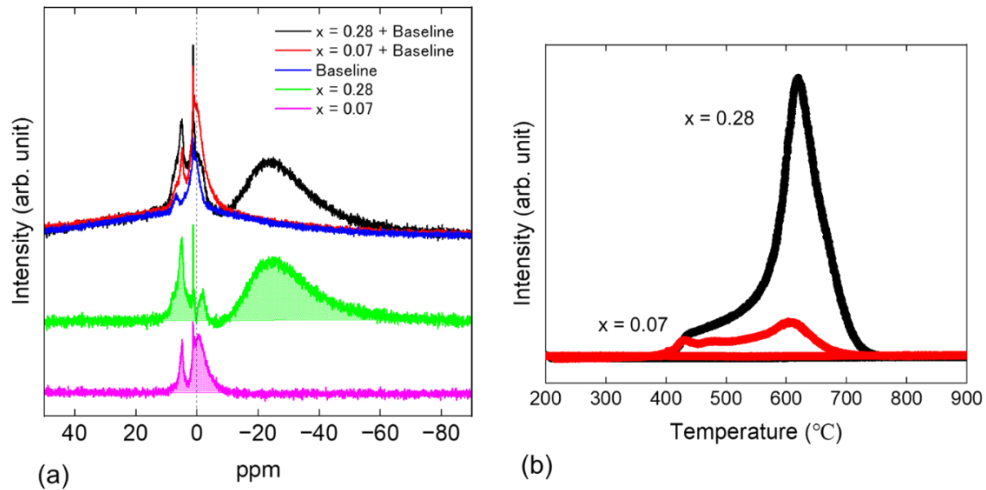


Figure S4. (a) ^1H NMR spectra of $\text{BaTiO}_{3-x}\text{H}_x$ ($x = 0.07$ and 0.28). (b) TPD-MS measurements for the same samples used for NMR measurements.

The valence and hydrogen content of the samples after HPDC were analyzed using ^1H NMR and TPD-MS. A chemical shift in the negative direction indicates an increase in electron density around hydrogen atoms, suggesting the formation of hydride (H^-). This change is attributed to charge neutrality compensation caused by oxygen vacancies, which is expected to induce the valence change in Titanium from $\text{Ti}^{4+} \rightarrow \text{Ti}^{3+}$ and promote hydrides (H^-) formation. The observed chemical shifts ranging from -1 ppm to -25 ppm reflect the increased electron density associated with decreasing oxygen concentration. In addition, the observed positive chemical shift, unrelated to hydrogen concentration changes, is likely due to surface hydroxyl group (OH), as discussed in a previous report [Ref. 24].

5. Change in hydrogen concentration along the thickness direction

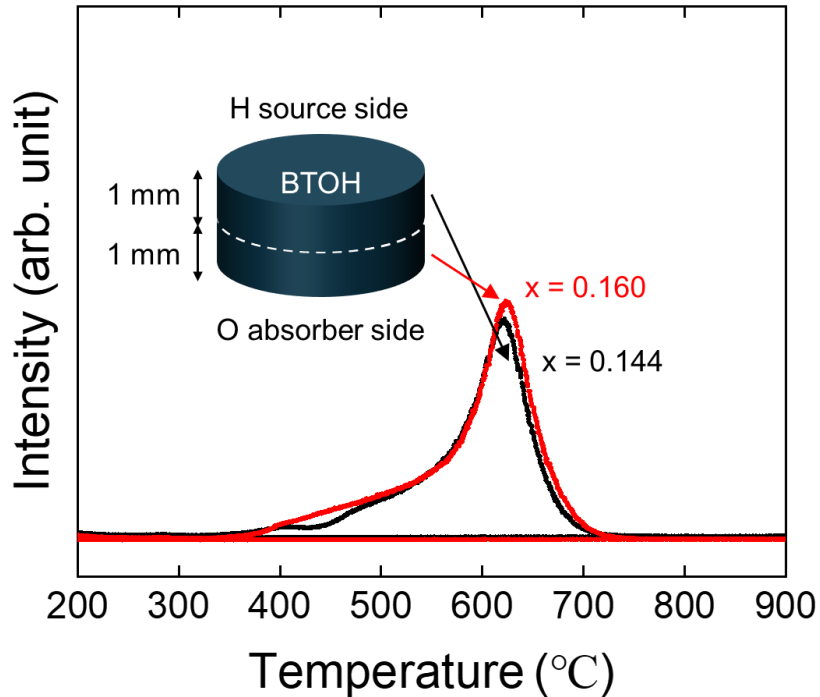


Figure S5. TPD-MS measurements for the upper and lower parts of the sample.

The as-prepared BTOH was cut into the upper side (hydrogen source side) and the lower side (oxygen absorber side), as illustrated in the inset of Figure S5. The hydrogen concentration in each part was then measured and similar profiles were observed. While the hydrogen content in the lower side was slightly higher than that in the upper side, assuming a linear gradient, the difference between them was estimated to be approximately $\delta x = 0.008$. This estimation was based on a sample thickness of 0.5 mm and an average hydrogen concentration of $x = 0.152$. Therefore, the shaped samples with a thickness of 0.5 mm, used for resistivity measurements, were considered to have an almost uniform hydrogen distribution.

6. XRD measurements

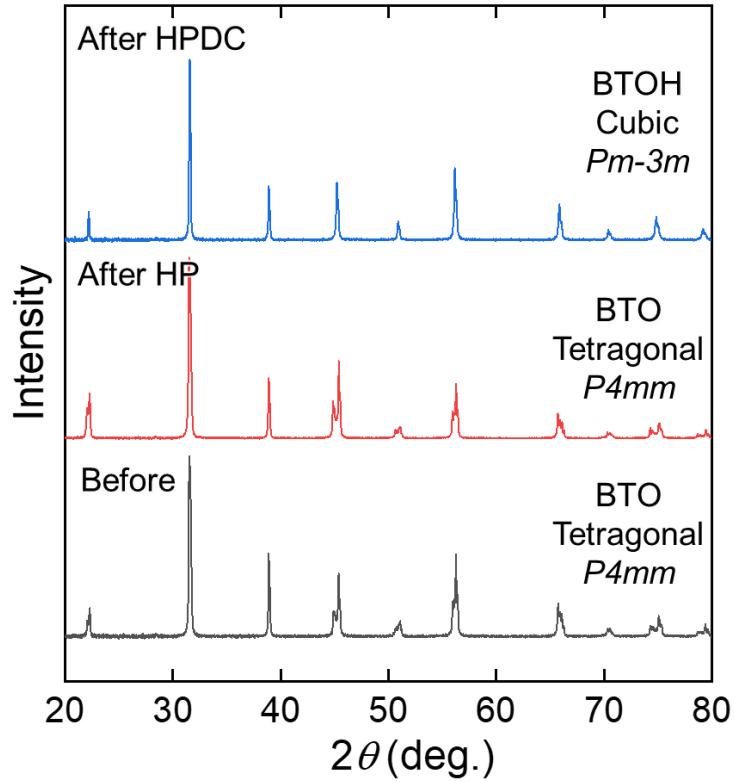


Figure S6. XRD measurements for the as-grown BaTiO_3 , BaTiO_3 after high-pressure (HP) treatment, and $\text{BaTiO}_{3-x}\text{H}_x$ after high-pressure diffusion control (HPDC).

The pressure and temperature conditions were identical for both HP and HPDC processes. This indicates that the structural change from the tetragonal to the cubic phase is driven by hydrogen substitution rather than the application of pressure.

7. Rietveld refinement analyses of powder neutron diffraction

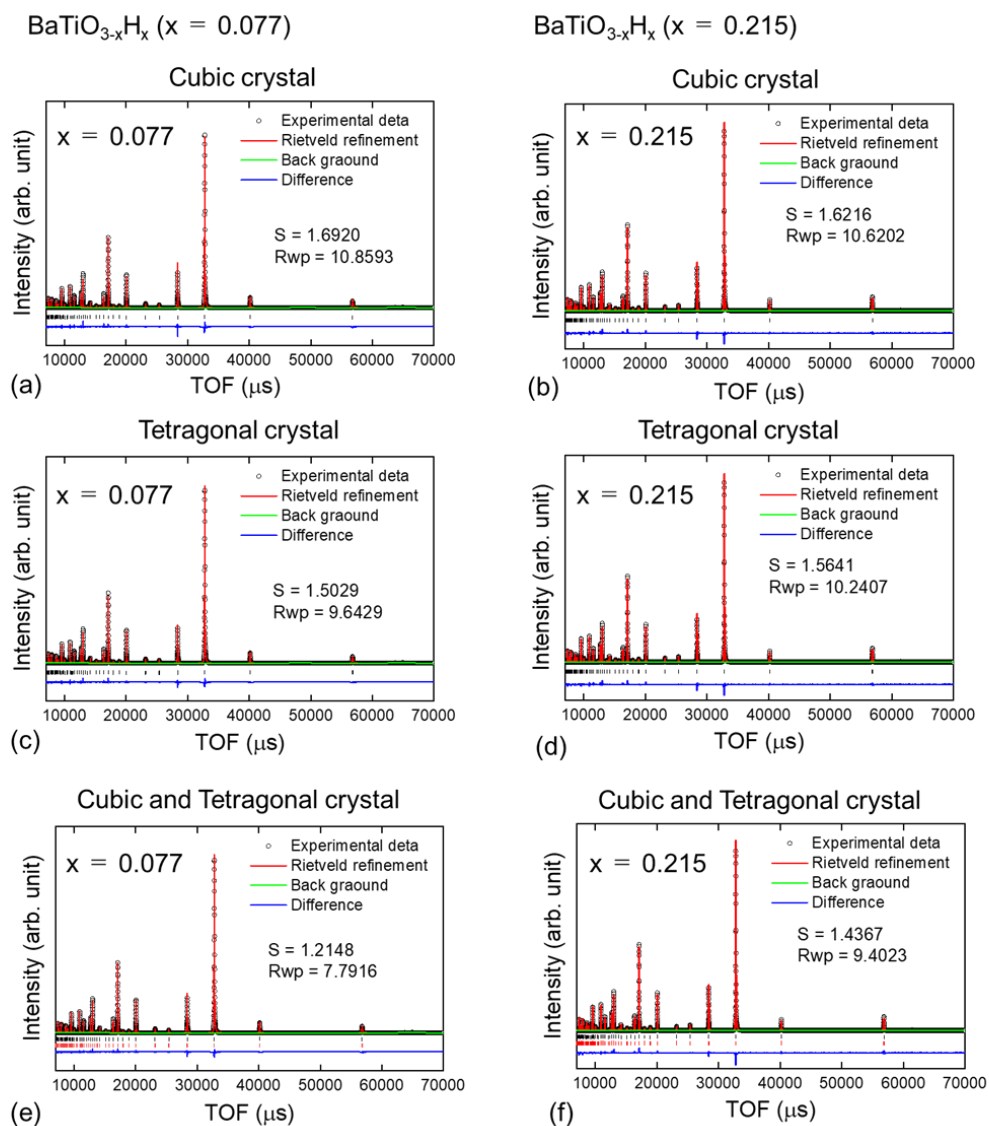


Figure S7. Rietveld refinement analyses of BaTiO_{3-x}H_x (x = 0.077 and 0.215) assuming (a, b) cubic phase, (c, d) tetragonal phase, and (e, f) their mixing phases.

Table S1. Structural parameters of BaTiO_{3-x}H_x (x= 0.077)

BaTiO _{3-x} H _x (x = 0.077)	Atom	Site	x/a	y/b	z/c	Occ.	B
<i>Pm-3m</i> (Cubic) a = 4.006036(4) x = 0.066	Ba	1a	0	0	0	1	0.147(10)
	Ti	1b	0.5	0.5	0.5	1	0.402(11)
	O	3c	0.5	0.5	0	0.9747(9)	0.282(5)
	H	3c	0.5	0.5	0	0.0221(13)	0.282(5)
S = 1.6920, Rwp = 10.8593%, RB = 3.5062%, RF = 5.0673%							
<i>P4mm</i> (Tetragonal) a = 4.004489(10) c = 4.00927(2) x = 0.071	Ba	1a	0	0	0.0370(13)	1	0.16(3)
	Ti	1b	0.5	0.5	0.539(5)	1	0.444(18)
	O1	2c	0.5	0	0.5447(6)	0.9738(9)	0.295(9)
	H1	2c	0.5	0	0.5447(6)	0.0235(14)	0.295(9)
	O2	1b	0.5	0.5	0.043(2)	0.9738(9)	0.295(9)
	H2	1b	0.5	0.5	0.043(2)	0.0235(14)	0.295(9)
S = 1.5029, Rwp = 9.6429, RB = 3.4977%, RF = 5.1757%							
2 phases		Weight ratio (Cubic ^a : Tetragonal ^b = 0.511(7) : 0.489(6))					
<i>Pm-3m</i> (Cubic) ^a a = 4.006094(7) x = 0.065	Ba	1a	0	0	0	1	0.151(14)
	Ti	1b	0.5	0.5	0.5	1	0.423(15)
	O	3c	0.5	0.5	0	0.9730(9)	0.292(6)
	H	3c	0.5	0.5	0	0.0217(4)	0.292(6)
<i>P4mm</i> (Tetragonal) ^b a = 4.00201(4) c = 4.01383(6) x = 0.065	Ba	1a	0	0	0.0170(0)	1	0.151(14)
	Ti	1b	0.5	0.5	0.517(14)	1	0.423(15)
	O1	2c	0.5	0	0.513(6)	0.9730(9)	0.292(6)
	H1	2c	0.5	0	0.513(6)	0.0217(4)	0.292(6)
	O2	1b	0.5	0.5	0.014(10)	0.9730(9)	0.292(6)
	H2	1b	0.5	0.5	0.014(10)	0.0217(4)	0.292(6)
S = 1.2148, Rwp = 7.7916%, RB ^a = 3.9003%, RF ^a = 4.4698%, RB ^b = 4.1740%, RF ^b = 6.2630%							

Constraint conditions: the use of identical isotropic atomic displacement parameters (B) for oxygen and hydrogen sites, uniform occupancy among hydrogen sites, and uniform occupancy among oxygen sites

Table 2. Structural parameters of BaTiO_{3-x}H_x (x= 0.215)

BaTiO _{3-x} H _x (x = 0.215)	Atom	Site	x/a	y/b	z/c	Occ.	B
<i>Pm-3m</i> (Cubic) a = 4.009636(3) x = 0.222	Ba	1a	0	0	0	1	0.168(9)
	Ti	1b	0.5	0.5	0.5	1	0.442(10)
	O	3c	0.5	0.5	0	0.9264(7)	0.247(4)
	H	3c	0.5	0.5	0	0.0739(11)	0.247(4)
S = 1.6216, Rwp = 10.6202%, RB = 4.9990%, RF = 5.5331%							
<i>P4mm</i> (Tetragonal) a = 4.008671(12) c = 4.01165(3) x = 0.204	Ba	1a	0	0	0.0344(19)	1	0.228(11)
	Ti	1b	0.5	0.5	0.524(2)	1	0.38(4)
	O1	2c	0.5	0	0.5441(4)	0.9263(8)	0.226(7)
	H1	2c	0.5	0	0.5441(4)	0.0680(12)	0.226(7)
	O2	1b	0.5	0.5	0.0414(12)	0.9263(8)	0.226(7)
	H2	1b	0.5	0.5	0.0414(12)	0.0680(12)	0.226(7)
S = 1.5641, Rwp = 10.2407%, RB = 5.1702%, RF = 6.0081%							
2 phases		Weight ratio (Cubic ^a : Tetragonal ^b = 0.651(12) : 0.349(12))					
<i>Pm-3m</i> (Cubic) ^a a = 4.009538(6) x = 0.213	Ba	1a	0	0	0	1	0.164(13)
	Ti	1b	0.5	0.5	0.5	1	0.392(13)
	O	3c	0.5	0.5	0	0.9240(8)	0.237(6)
	H	3c	0.5	0.5	0	0.0715(12)	0.237(6)
<i>P4mm</i> (Tetragonal) ^b a = 4.00752(6) c = 4.01611(14) x = 0.213	Ba	1a	0	0	0.0464(19)	1	0.164(13)
	Ti	1b	0.5	0.5	0.5207(16)	1	0.392(13)
	O1	2c	0.5	0	0.5455(17)	0.9240(8)	0.237(6)
	H1	2c	0.5	0	0.5455(17)	0.0715(12)	0.237(6)
	O2	1b	0.5	0.5	0.052(2)	0.9240(8)	0.237(6)
	H2	1b	0.5	0.5	0.052(2)	0.0715(12)	0.237(6)
S = 1.4374, Rwp = 9.4075%, RB ^a = 5.0309%, RF ^a = 4.7957%, RB ^b = 6.2275%, RF ^b = 10.7327%							

Constraint conditions: the use of identical isotropic atomic displacement parameters (B) for oxygen and hydrogen sites, uniform occupancy among hydrogen sites, and uniform occupancy among oxygen sites

8. Possibility of OH formation

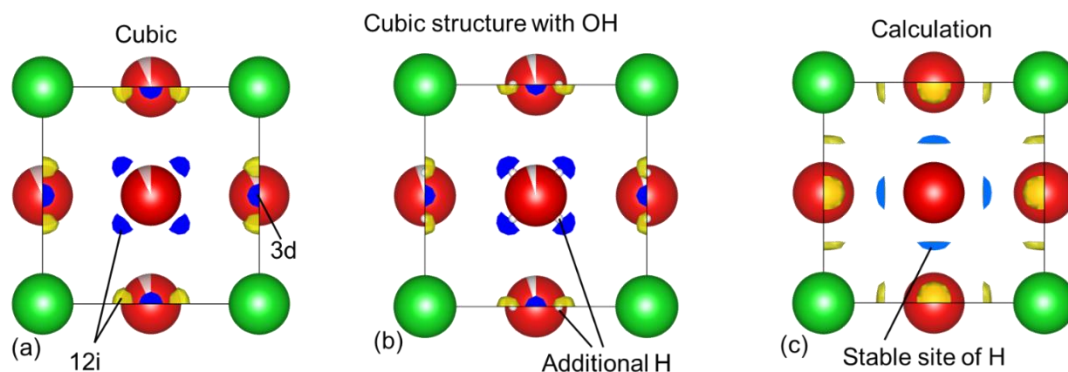


Figure S8. (a) MEM analysis assuming cubic structure. The negative scattering densities are indicated by yellow and blue. (b) MEM analysis assuming cubic structure with OH. (c) DFT calculation for the stable hydrogen position.

Table S3 Structural parameters of $\text{BaTiO}_{3-x}\text{H}_x(\text{OH})_y$ ($x = 0.215$)

$\text{BaTiO}_{3-x}\text{H}_x$ ($x = 0.215$)	Atom	Site	x/a	y/b	z/c	Occ.	B
$Pm-3m$ (Cubic)	Ba	1a	0	0	0	1	0.120(9)
$a = 4.009631(3)$	Ti	1b	0.5	0.5	0.5	1	0.452(10)
$x = 0.619$	O	3c	0.5	0.5	0	0.9661(16)	0.448(8)
	H	3c	0.5	0.5	0	0.030(2)	0.448(8)
	H	12i	0	0.6029(14)	0.6029(14)	0.0441(10)	0.448(8)
S = 1.4598, Rwp = 9.5592%, RB = 3.1812%, RF = 4.8882%							

In Figure S8(b), additional hydrogen was assumed to occupy the 12i site, as listed in Table S3. Although the Rwp converged to 9.5592%, the estimated hydrogen concentration was ($x = 0.619$) inconsistent with the TPD-MS results. Moreover, DFT calculations indicated that the 12j site was more favorable for hydrogen than the 12i site, as shown in Figure S8(c). The same calculation techniques in [Ref. 27] was used to identify the most stable hydrogen position.

9. Methods

Experimental procedures

BaTiO₃ powder (Purity 98%, FUJIFILM Wako Pure Chemical Corp.), YSZ powder (Purity 99%, FUJIFILM Wako Pure Chemical Corp.), MgH₂ powder (Purity 70%, FUJIFILM Wako Pure Chemical Corp.), and Ti powder (Purity 98%, FUJIFILM Wako Pure Chemical Corp.) were used for each pellets in sample space. The high-pressure cells (C & T Factory) with a diameter of $\phi 4.2$ mm for sample space were modified for HPDC as reported in [Ref. 17]. A high-pressure apparatus (CTF-MA180P, C & T Factory) was used to apply pressure and adjust temperature. XRD measurements (Rigaku MiniFlex600 with D/teX Ultra) were performed to identify the crystalline phase in Figure S5. TPD measurements (MictotracBEL Corp. BELMASS) were performed to estimate the H concentration. The temperature dependence of the sample resistivity was measured using a refrigeration system (Thermal Block Company, SB-1.5KCRS0.5-TRB). The samples, measuring $4.2 \times 1 \times 1.5$ mm³, were prepared, and Ag paste was used to contact the gold electrode with the samples. The four-probe method was used to measure the electrical resistivity. The time-of-flight (TOF) powder neutron diffraction was measured in BL-20 at the Material and Life Science Experimental Facility (MLF) of the Japanese Proton Accelerator Research Complex (J-PARC). Rietveld refinements for TOF powder ND data were performed using the program Z-Rietveld [Ref. 25]. Although the hydrogen in BTOH was not substituted for deuterium, the background was sufficiently small, and high-quality diffraction data with a high S/N ratio were obtained. The chemical state of H was measured by ¹H magic angle spinning (MAS) NMR using a spectrometer (Bruker AVANCE III HD 600WB) at a Larmor frequency of 600.395 MHz. A Bruker MAS probe head (MAS1.3DR) was used with a MAS rotor with 1.3 mm diameter (HZ14752). The sample was packed into the rotor, and the spin rate was 60 kHz. The ¹H chemical shifts were referenced to TMS at 0 ppm. Adamantane was used as a second reference material, the central signal of which was set at 1.83 ppm.

DFT Calculations

Energy landscapes for Hydrogen (H) in a BaTiO₃ unit cell were calculated. The projector augmented wave method, implemented in the Vienna *ab initio* simulation package[Ref. 28] and the generalized gradient approximation (Perdew–Burke–Ernzerhof approximation[Ref. 29]) as the exchange-correlation functional were employed. The plane-wave cutoff energy was set to 300 eV. The Brillouin zone was sampled using a $5 \times 5 \times 5$ Monkhorst-pack grid, and Gaussian smearing with $\sigma = 0.04$ was applied. The energetic local minimum for H was identified by exploring energy landscapes, which

involved calculating the total energies of the unit cell (BaTiO_3) with an additional H atom placed at different positions. The H position was varied across the entire unit cell, with a pitch of approximately 0.1 \AA along each axis, resulting in about 64,000 configurations. The same method was used in a previous study [Ref. 27].